Evidence of convective constraint release during hole growth in freely standing polystyrene films at low temperatures

C. B. Roth, B. Deh, B. G. Nickel, and J. R. Dutcher
Department of Physics and the Guelph-Waterloo Physics Institute, University of Guelph, Guelph, Ontario, Canada N1G 2W1
(Received 16 July 2004; revised manuscript received 25 April 2005; published 10 August 2005)

Hole growth measurements were performed using optical microscopy on freely standing polystyrene films at temperatures that were slightly larger than the bulk value of the glass transition temperature T_g^{bulk}. For the measured range of temperatures, we have observed a transition from linear growth of the hole radius R during the early stages to exponential growth of R at later times. We have characterized this transition as a function of molecular weight $120\times10^3<M_w<2240\times10^3$, film thickness 61 nm$<h<$125 nm, and temperature 101 °C $<T<$117 °C. The viscosity at the edge of the hole inferred from the long time exponential growth regime exhibits shear thinning due to the large shear strain rates present at the edge of the hole. The $R(t)$ data for all times can be fit very well using an expression that describes exponential hole growth with a time-dependent viscosity that allows for an initial, transient response due to the decay of elastic entanglements. The time scale for the decay of the transient behavior is interpreted in terms of the decay of entanglements by the convective constraint release mechanism of the tube theory of entangled polymer dynamics.

DOI: 10.1103/PhysRevE.72.021802 PACS number(s): 68.15.+e, 68.60.Dv, 83.60.Fg

I. INTRODUCTION

Understanding the dynamics of polymer chains in entangled polymer melts has been a major research focus and area of controversy over the last forty years. As of 1990, there were a number of competing theories for entangled polymer melts [1], however, theoretical efforts during the last decade have refined Doi and Edwards' original tube model [2–5], which included the concepts of the tube [6] and reptation [7], into an elaborate model which attempts to describe the motions of polymers of various architectures (linear, branched, etc.) in melts by including a number of different relaxation mechanisms that dominate for different polymer architectures and at different time scales.

The central feature of the Doi and Edwards (DE) model is a Langevin equation describing the motion of a single primitive chain confined to a tube, which is a mean-field theory. The primitive chain is comprised of effective segments that each represent a section of the real polymer chain, where each tube segment (modeled as a bead and spring) is essentially the distance between entanglement points and is large enough to have Gaussian coil properties. During the refinements to the theory, the basic Langevin equation from the DE model has been retained, with additional terms added to account for relaxation mechanisms other than reptation [8–10].

We briefly list the various relaxation mechanisms in the current version of the tube theory of entangled polymer dynamics and discuss their relative importance for monodisperse linear polymer chains in melts at different shear strain rates. The fastest relaxation, referred to as "chain retraction," occurs on a time scale of τ_R (the Rouse time) and corresponds to the primitive chain returning to its equilibrium length by the fast Rouse modes of the system when the tube is deformed by flow. The most well known relaxation mechanism, reptation, a one-dimensional Brownian motion diffusion along the contour length of the tube, is the slowest with time scale τ_d and only dominates in linear chains at very small strain rates ($\dot{\gamma}<\tau_d^{-1}$). Contour length fluctuations (CLFs) of the tube are stochastic breathing-mode retractions of the chain ends [11–15]. CLF is the dominant mode of relaxation in branched polymers where reptation is suppressed by the branching points. The addition of CLF to reptation was shown to give rise to the $\eta\sim M_w^{3.4}$ dependence [15]. Constraint release (CR) accounts for relaxation of the tube due to the disappearance of constraints, i.e., entanglement points, when the surrounding chains relax out of their tubes by reptation or CLF. CR is modeled by treating the entire tube as a Rouse chain which undergoes a "Rouse tube hop" when a constraint is released [16–18]. This mode of relaxation was thought to be only important for polydisperse systems where shorter chains would quickly reptate out of their tubes releasing the constraints surrounding the longer chains. A form of CR, referred to as convective constraint release (CCR), becomes important for shear strain rates larger than the reptation rate ($\dot{\gamma}>\tau_d^{-1}$) because entanglement points are swept away with the convection of surrounding chains by flow. The CR-generating events are no longer due to only reptation or CLF, but now occur also by the process of chain retraction. In CCR, the Rouse tube hops, which are assumed to act with an equal rate on all tube segments along the chain, are randomly oriented relative to the shearing direction using a noise term [19–24]. The rate of the CCR relaxation process follows the bulk deformation rate such that continuous relaxation of the tube contour is achieved however fast the flow. Finally, "chain stretch" is defined as a flow-induced increase in the primitive path length, which can be incorporated into the model with a term proportional to the local gradients in chain tension [25–30]. For moderately nonlinear flows ($\dot{\gamma}\ll\tau_R^{-1}$), affine deformation of the system is assumed as the overall length of the primitive chain remains constant due to the continuous readjustment by the fast Rouse modes (i.e., chain retraction). However, for shear strain rates comparable to or larger than the inverse of the

longest Rouse time τ_R ($\dot{\gamma} \geqslant \tau_R^{-1}$), this assumption is no longer true and chain stretch is believed to become important.

In the tube theory for entangled polymer dynamics, the dominant relaxation mechanism is determined by the magnitude of the shear strain rate $\dot{\gamma}$ relative to the reptation τ_d^{-1} and Rouse τ_R^{-1} rates [8,30,31]. In the low shear strain rate regime, $\dot{\gamma} < \tau_d^{-1}$, reptation is the dominant relaxation mechanism for linear polymers such that the material relaxes with a time scale τ_d. This is the well-known linear viscoelastic limit with constant viscosity η_0. In the intermediate shear rate regime $\tau_d^{-1} < \dot{\gamma} < \tau_R^{-1}$, CCR is the dominant relaxation mechanism occurring with a time scale of the order of $\dot{\gamma}^{-1}$. Nonlinear viscoelastic phenomena, such as shear thinning, occur in this regime. The high shear strain rate regime $\dot{\gamma} > \tau_R^{-1}$ is the least well understood at present; relaxations in this regime are believed to be attributed to chain stretching [30].

Shear thinning has been observed during the growth of holes in thin, freely standing polystyrene (PS) films [32]. Holes form in the films at elevated temperatures either due to nucleation by defects, e.g., dust or density inhomogeneities, or their formation can be driven by the dispersion or van der Waals interaction [33]. Unsupported or freely standing thin liquid films are inherently unstable: the symmetric geometry with air on both sides of the liquid film always results in attractive van der Waals forces which, for sufficiently thin films, tend to bring the two film surfaces together leading to the formation of a hole which, once formed, grows with time driven by surface tension. The driving force of surface tension can be balanced by inertia for the case of fluid soap films [34,35], for which material is observed to build up into a rim around the edge of the hole, or by viscous damping for the case of viscous fluid films [36], for which uniform thickening of the film is observed [32,37,38]. Viscoelastic materials such as polymers also have elastic properties that can become important at low temperatures [39–43].

Hole growth in freely standing viscous films is driven radially outward by a constant stress at the edge of the hole $\sigma = 2\epsilon/h$ due to surface tension. The flow has a constant velocity profile across the thickness of the film, referred to as plug flow, which only depends on the radial distance r from the center of the hole:

$$v(r) = \dot{R}R/r, \tag{1}$$

where the radial position R of the edge of the hole travels with velocity $dR/dt \equiv \dot{R}$. The rate of energy loss due to viscous dissipation within the film can be written as [37]

$$\dot{E}_{\mathrm{kin}}(r) = 2\eta \int_R^\infty 2\pi r h dr \left[\left(\frac{\partial v}{\partial r} \right)^2 + \left(\frac{v}{r} \right)^2 \right] = 4\pi \eta h \dot{R}^2, \tag{2}$$

where h is the film thickness and η is the viscosity. $\dot{E}_{\mathrm{kin}}$ is balanced by the gain in surface energy per unit time

$$\dot{E}_{\mathrm{surf}}(r) = (2\epsilon) 2\pi R \dot{R}, \tag{3}$$

as determined by the surface tension ϵ. Equating Eqs. (2) and (3) yields

$$\frac{\dot{R}}{R} = \frac{\epsilon}{\eta h}, \tag{4}$$

corresponding to exponential growth of the hole radius as a function of time:

$$R(t) = R_0 \exp(t/\tau), \tag{5}$$

where the characteristic growth time τ is related to the material constants by

$$\tau = \frac{\eta h}{\epsilon}. \tag{6}$$

Since the film thickness h can be measured independently using, e.g., ellipsometry, and the surface tension ϵ is not expected to differ from that in bulk because h is large compared with the length scale associated with surface tension ($\sim$1 nm [44]), the hole growth experiment provides a simple and elegant technique for measuring the viscosity at the edge of the hole.

With decreasing film thickness h, the stress at the edge of the hole increases as $\sigma = 2\epsilon/h$, which results in an increase in the shear strain rate $\dot{\gamma}$ given by [32]

$$\dot{\gamma} = \frac{2\dot{R}}{R} = \frac{2}{\tau}. \tag{7}$$

In a study of hole growth in thin, freely standing PS films, with molecular weight $M_w = 767 \times 10^3$, measured at a temperature 18 °C greater than the bulk value of T_g [32], it was found that the viscosity η at the edge of the hole decreased with increasing $\dot{\gamma}$ in agreement with the bulk nonlinear viscoelastic phenomenon of shear thinning, according to the power law

$$\eta(\dot{\gamma}) \sim |\dot{\gamma}|^{-d} \tag{8}$$

with an exponent of $d = 0.65 \pm 0.03$ that was slightly smaller than the bulk value of $d \sim 0.8$ [45].

In the present manuscript, we demonstrate that the thin film geometry is also ideal for testing aspects of the tube theory of entangled polymer dynamics. We present optical microscopy measurements of hole growth in freely standing polystyrene (PS) films that extend the range of previous hole growth studies in freely standing PS films [32,43,46,47] to small holes in very thin films ($h \approx 100$ nm) at low temperatures (slightly larger than the bulk glass transition temperature of polystyrene, $T_g^{\mathrm{bulk}} = 97$ °C). In measurements of the hole radius R as a function of time, we have observed a transition from linear growth of the hole radius during the early stages of hole growth to exponential growth at later times. We have characterized the transition from linear to exponential hole growth experimentally as a function of molecular weight ($120 \times 10^3 < M_w < 2240 \times 10^3$), film thickness (61 nm $< h <$ 125 nm), and temperature (101 °C $< T <$ 117 °C). Empirically, we find that excellent fits to the $R(t)$ data can be obtained using an expression for $R(t)$ that corresponds to a viscous fluid model incorporating a time-dependent viscosity $\eta(t)$. The expression for $R(t)$ is appealing since it contains only three fitting parameters, each of

which has a physical meaning: R_0, the hole radius at the beginning of the hole growth experiment; τ, a characteristic growth time for exponential hole growth at long times; and τ_1, a time scale which we ascribe to the decay of entanglements of the molecules during the initial stages of hole growth.

Perhaps it is not surprising that the dynamics of flow in very thin polymer films can be complex due to the large stress imposed by surface tension at the edge of the growing hole. This can lead to highly nonlinear viscoelastic behavior and provide a new experimental window into the complexities of nonlinear viscoelastic flow that have been revealed theoretically by recent advances in the tube theory of entangled polymer dynamics. To date, this theory has outpaced the availability of good experimental data obtained at high shear rates to test the complexities of the theory [8,48], as well as the large number of constitutive equations available [49]. The data obtained in the present hole growth experiments, with a relatively simple experimental geometry, corresponding to radial plug flow of the polymer molecules, should provide a good test case of the available theories for monodisperse linear polymer chains in an entangled melt at high shear rates. In our experiments, we find that the values of τ_1 obtained in our fits to the $R(t)$ data are consistent with chain disentanglement via the convective constraint release (CCR) mechanism of the tube theory of entangled polymer dynamics. In addition, in the late stages of hole growth, corresponding to exponential growth of the hole radius [see Eq. (5)], the measured viscosity values are consistent with the bulk phenomenon of shear thinning. A complete compilation of shear thinning results obtained for freely standing PS films is given in Ref. [47].

II. EXPERIMENT

Thin freely standing polystyrene (PS) films were prepared using monodisperse atactic polystyrene, obtained from Polymer Source, Inc. A series of four molecular weight values ranging from $M_w=120\times10^3$ to 2240×10^3 were used (see Table I for sample details). Polymer films were spincoated at 4000 rpm onto freshly cleaved mica substrates from dilute solutions of PS dissolved in toluene with concentrations between 1.4 and 2.3 % of PS by mass to produce film thicknesses h between 61 and 125 nm. All PS films on mica were heated under vacuum to $T=115$ °C for 12 h to remove any trapped solvent, and subsequently cooled to room temperature at less than 1 °C/min to produce samples with a well defined and reproducible thermal history. The PS films were transferred onto a clean (Milli-Q, resistance >18 MΩ) water surface, and then transferred onto stainless steel sample holders containing a 4-mm diameter hole, resulting in freely standing PS films that were dried in air [50]. Pieces of the same PS films were also transferred onto clean silicon wafers for a determination of the PS film thicknesses to within ±1 nm using ellipsometry.

The freely standing PS films were heated in a custom-built hot stage on an Olympus BX-60 optical microscope and measurements of the hole radius R as a function of time t were obtained by capturing a time sequence of optical micrographs, and digitally measuring the area of the hole in each micrograph with image analysis software (ImagePro Plus by Media Cybernetics) from which the hole radius R was calculated. For the measurements, the PS freely standing films were heated quickly at a rate of 5–10 °C/min to the measurement temperature between 101 and 117 °C, and held at the elevated temperature while hole formation and growth occured. The measurement time varied from ~30 min at the highest temperatures to many hours for the lowest temperatures. Measurements of the hole radius were begun as soon as a hole was identified, with initial hole radii values that were typically 1 μm.

TABLE I. Molecular weight M_w, polydispersity index M_w/M_n, and film thickness h of polystyrene samples studied along with the measurement temperatures T used for each set of films. The uncertainty quoted for each film thickness value is the standard deviation of values measured for the set of films with the same nominal thickness.

PS $M_w(\times10^3)$	M_w/M_n	Film thickness[a] h (nm)	Measurement temperature T(°C)
120	1.04	77±1	101, 103, 105, 107
282	1.07	94±1	101, 103, 107
717	1.12	61±3, 90±3, 125±4	101, 103, 105, 107, 110, 112, 115, 117
2240	1.08	83±3	101, 103, 105, 107, 110, 112, 115

[a]All films have the bulk value of the glass transition temperature $T_g^{\text{bulk}}=97$ °C for polystyrene, except for the $h=61$ nm films of $M_w=717\times10^3$, which have a $T_g=80$ °C [74].

III. RESULTS AND ANALYSIS

A. Time dependence of the hole radius

Measurements of the radius $R(t)$ of individual holes in freely standing PS films revealed a transition from a linear dependence of the hole radius on time, observed at early times, to an exponential dependence of the hole radius on time, observed at later times. In Fig. 1 are shown the $R(t)$ data collected for a PS freely standing film of $M_w=2240\times10^3$ and thickness $h=79$ nm held at a temperature of $T=103$ °C. By plotting the $R(t)$ data using both linear [Fig. 1(a)] and natural logarithmic [Fig. 1(b)] axes for the R values, it can be seen that initially the hole radius grows linearly with time before changing to an exponential time dependence at later times.

The data set shown in Fig. 1 is representative of all of the data sets collected for the set of samples used in the present study (see Table I). The period of time corresponding to the initial linear growth behavior decreased with decreasing molecular weight M_w and increasing temperature, such that only exponential growth was observed for films with the lowest value of $M_w=120\times10^3$ at all temperatures measured (101 °C$<T<$107 °C) and for films with $M_w=282\times10^3$ at the highest temperature measured ($T=107$ °C). All of the films measured in the present study exhibited exponential

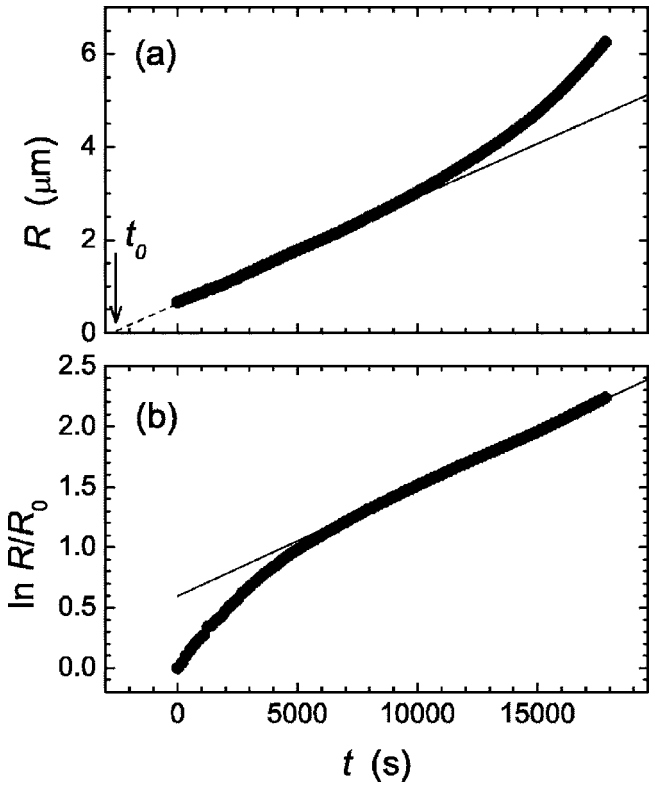

FIG. 1. Hole radius $R(t)$ data for a freely-standing PS film of $M_w=2240\times10^3$ and $h=79$ nm held at $T=103$ °C with (a) linear and (b) natural logarithmic axes for the R values. The straight solid lines in the plots correspond to best fits to (a) $R(t)=vt+c$, with $v=0.23$ nm/s and $c=0.63$ μm, for $0<t<7740$ s and (b) $R(t)=Ae^{t/\tau}$, with $\tau=10900$ s and $A=1.21$ μm, for $8100\text{ s}<t<17820$ s. The dashed line in part (a) corresponds to the extrapolation of the best linear fit of the R versus t data to $R=0$ at $t=t_0$.

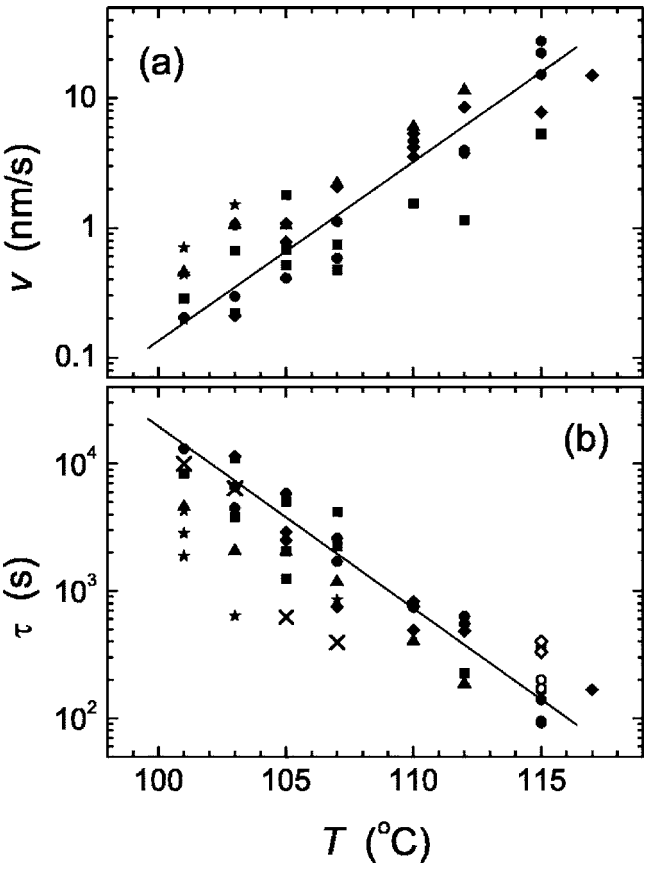

FIG. 2. (a) Velocity v of the linear growth regime observed at early times and (b) characteristic growth time τ of the exponential growth regime observed during the late stages of hole growth, as a function of temperature T. In the two graphs, the symbols corresponding to a given data set are the same: $M_w=120\times10^3$, $h=77$ nm (×); $M_w=282\times10^3$, $h=94$ nm (★); $M_w=717\times10^3$, $h=61$ nm (▲); $M_w=717\times10^3$, $h=90$ nm (●); $M_w=717\times10^3$, $h=125$ nm (♦); and $M_w=2240\times10^3$, $h=83$ nm (■). In part (b) data from Ref. [32] collected at $T=115$ °C have been added: $M_w=767\times10^3$, $h=96$ nm (○); and $M_w=767\times10^3$, $h=122$ nm (◇).

growth of the hole radius for very long times.

We note that the linear growth portion of the $R(t)$ data does not correspond to the leading, linear term in a series expansion of an exponential function of time. Even if the characteristic exponential growth time τ were very large, exponential growth would correspond to a straight line on a plot of $\ln R$ versus t, and this is not observed for hole growth experiments in which a linear growth portion of the $R(t)$ data was observed (see, e.g., Fig. 1).

The initial portion of the data sets, for which linear growth was observed, was fit to an equation for a straight line of the form $R(t)=vt+c$ to obtain the velocity v. The late stage data were fit to an equation for exponential growth of the form $R(t)=Ae^{t/\tau}$ to obtain the characteristic growth time τ. The ranges of data points used for the fits to the linear and exponential growth equations were chosen such that the deviations of the ordinate values from the best fit straight line on the R versus t plot and the $\ln(R/R_0)$ versus t plot were less than 1.5% of the ordinate range. Figure 2 shows the best fit v and τ values plotted as a function of temperature for all of the samples measured in this study. Both the v and τ values depend strongly on temperature; the strong temperature dependence of τ is expected from Eq. (6), given the strong temperature dependence of the viscosity η. There is no significant dependence of the v and τ values on M_w. The τ values measured at $T=115$ °C in the present study are in agreement with those reported in Ref. [32] for hole growth measurements of PS films of $M_w=767\times10^3$ at $T=115$ °C for film thicknesses $h=96$ nm and 122 nm [see Fig. 2(b)].

Before discussing the interesting transition from linear to exponential growth as time proceeds, we first analyze the late stage data corresponding to exponential growth. From the characteristic growth time τ, we calculated the corresponding viscosity η at the edge of the hole using Eq. (6) and the shear strain rate $\dot{\gamma}$ using Eq. (7). A plot of η/η_0 versus the reduced shear strain rate [45]

$$\beta=\frac{\eta_0 M_w\dot{\gamma}}{\rho R_{\text{mol}}T} \tag{9}$$

is shown in Fig. 3, where R_{mol} is the molar gas constant, and ρ is the mass density. The details of the calculation of the η/η_0 and β values are given in Ref. [47]. In Fig. 3, we have

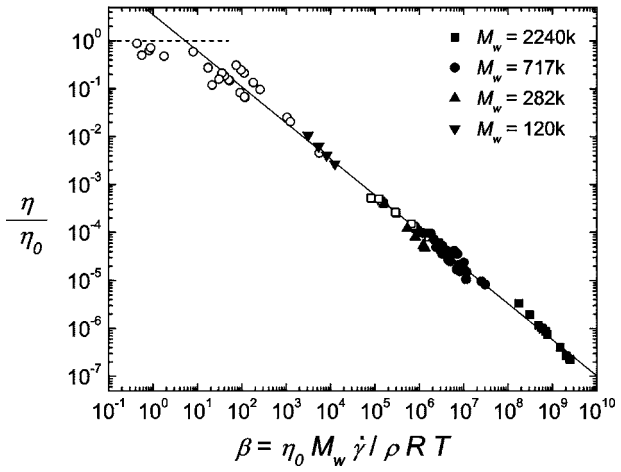

FIG. 3. Viscosity η at the edge of the hole determined from hole growth measurements of freely standing PS films at temperatures close to and above T_g^{bulk}, divided by the zero shear rate viscosity η_0, as a function of the reduced shear strain rate $\beta=\eta_0 M_w \dot{\gamma}/\rho RT$ for M_w values of 120×10^3 (▼), 282×10^3 (▲), 717×10^3 (●), and 2240×10^3 (■). The solid line is the best fit of the $\log_{10}(\eta/\eta_0)$ versus $\log_{10}\beta$ data from the present study (solid symbols) to a straight line with a slope of -0.75 ± 0.01. Data from previous studies are also shown: Ref. [32] (□), and Ref. [43] (○).

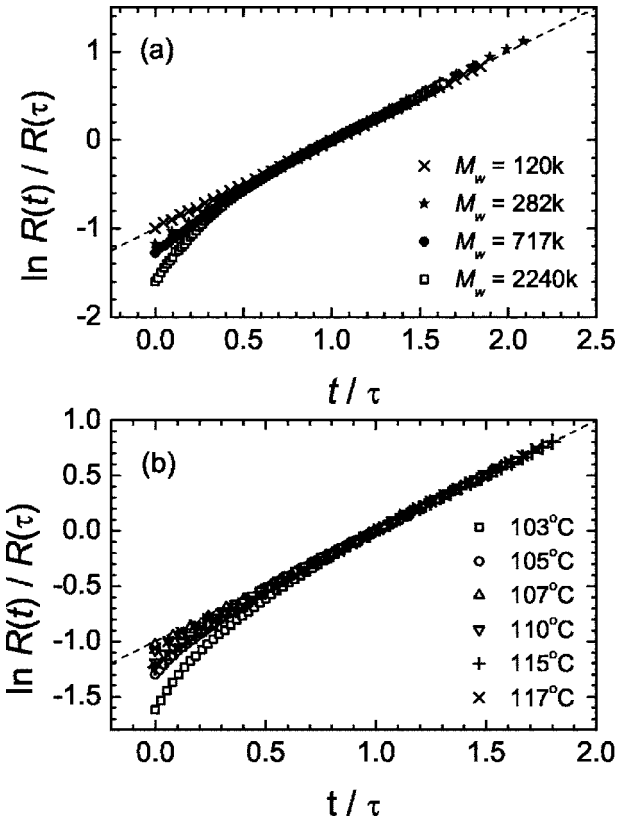

FIG. 4. Plots of $\ln[R(t)/R(\tau)]$ versus t/τ for films (a) measured at the same temperature ($T=103$ °C) with different M_w values: $M_w=120\times10^3$ and $h=78$ nm, $M_w=282\times10^3$ and $h=94$ nm, $M_w=717\times10^3$ and $h=91$ nm, and $M_w=2240\times10^3$ and $h=79$ nm and (b) measured at different temperatures with the same M_w value ($M_w=717\times10^3$) and thickness ($h=125$ nm).

also included data collected in previous studies of hole growth in freely standing PS films [32,43].

The large β values obtained in the present study ($3\times10^3<\beta<3\times10^9$) indicate that the hole growth measurements correspond to the nonlinear regime $\beta>10$ [45], in which shear thinning effects (characterized by decreasing η with increasing β) dominate. It is interesting to note that the data of Ref. [43], obtained for thicker films at higher temperatures than in the present study, extend the range of the data in Fig. 3 from the nonlinear regime to the linear regime, corresponding to $\eta=\eta_0$ which indicates that hole growth is a shear deformation, and not an extensional deformation since the steady state extensional viscosity at small strain rates, the Trouton viscosity, is three times the zero shear viscosity η_0. A detailed discussion of all shear thinning results obtained to date for freely standing PS films is given in Ref. [47].

We now focus on the observed transition from linear to exponential hole growth as time proceeds (see Fig. 1). In Fig. 4 are shown two plots of $\ln[R(t)/R(\tau)]$ versus time t/τ: (a) for constant temperature and different M_w values and (b) for constant M_w and film thickness at different temperatures. The normalization of the $R(t)$ values by $R(\tau)$ and the t values by τ scales the data such that the data sets coincide for $t=\tau$, and the long time portions of the data, which exhibit exponential growth, overlap. From the plots shown in Fig. 4, it can be seen that the largest deviations from exponential growth at small times ($t/\tau<1$) occur for the higher M_w films [Fig. 4(a)] and at the lower temperatures [Fig. 4(b)]. The transient behavior observed during the initial stages of hole growth was isolated by subtracting the straight dashed lines in Fig. 4, representing exponential growth, from each data set. The transient behavior, defined as

$$\ln[R(t)/R(\tau)]-(t/\tau-1) \tag{10}$$

is plotted as a function of the reduced time t/τ in Figs. 5(a) and 5(b) for the data sets displayed in Figs. 4(a) and 4(b), respectively. The transient behavior was found to be well described by an exponential decay with a single characteristic time τ_1 as shown by the fit to the $T=103$ °C data set in Fig. 5(b). This analysis suggests that the linear behavior observed during the early stages of growth is the result of the exponential decay of a transient effect.

The origin of the time scale, $t=0$, in Figs. 1, 4, 5(a), and 5(b) corresponds to the start of each experiment, i.e., the time at which the first optical micrograph was collected after identifying a hole in the film using the optical microscope. Since holes were identified with different initial sizes, $t=0$ corresponds to different initial radii. To compare the different data sets, it is sensible to shift the measured time values to refer each data set to a common initial radius. We have chosen to refer the data sets to the time $t=t_0$ corresponding to $R(t_0)=0$ by extrapolating the linear fits to the initial portion of the $R(t)$ data sets to $R=0$ [see Fig. 1(a)]. The value of $R=0$ never occurs in practice, since there is a minimum critical hole radius $R_c=h/2$ above which holes must form for nucleated holes to grow with time [51], but this provides a convenient common reference point. In Figs. 5(c) and 5(d) are

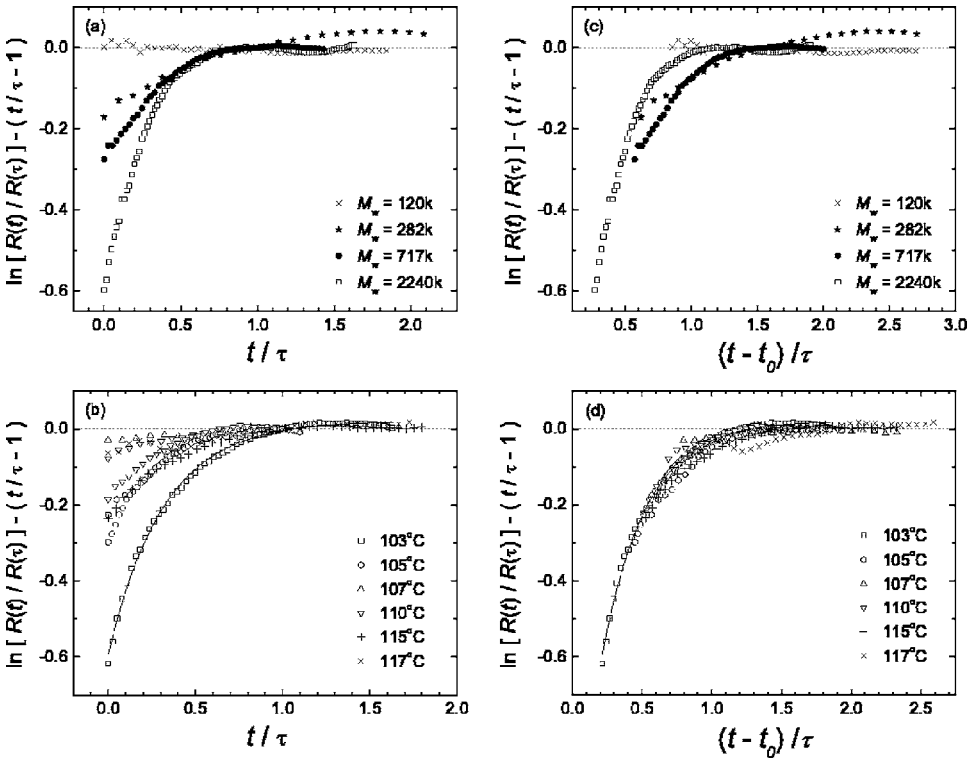

FIG. 5. Plots of the transient $\ln[R(t)/R(\tau)]-(t/\tau-1)$ versus t/τ for (a) the same data set as in Fig. 4(a), and (b) the same data set as in Fig. 4(b). Parts (c) and (d) correspond to the same data sets as in parts (a) and (b), respectively, referenced to a common extrapolated starting time t_0 corresponding to $R(t_0)=0$. The solid curves in parts (b) and (d) were calculated as the best fit of the $T=103$ °C data set to a single exponential decay $Be^{-(t-t_0)/\tau_1}$ with $\tau_1=0.316\tau=3610$ s.

shown the data sets from Figs. 5(a) and 5(b) shifted in time by the amount t_0 and normalized by τ. Reasonable overlap of the different data sets is obtained in Figs. 5(c) and 5(d) which provides strong evidence that the transient behavior is caused by the same mechanism in all of the films and is well described by a single exponential decay $Be^{-(t-t_0)/\tau_1}$ with a time scale τ_1 that is proportional to the hole growth time τ [see Figs. 5(b) and 5(d)].

Although it is possible to analyze the early stage and late stage hole growth data separately, as shown in Figs. 1–5, it is better to have a single fitting function for the $R(t)$ data that is valid for all times measured in the experiment. Ideally, the fitting function should have a small number of fitting parameters, each of which has a physical significance. Based on the identification of an initial transient behavior that decays exponentially with time [see Figs. 5(b) and 5(d)], we have found empirically that the following function describes the $R(t)$ data well for all of the films used in the present study:

$$R(t) = R_0 \exp\left[\frac{t}{\tau}[1+\exp(-t/\tau_1)]\right]. \tag{11}$$

Equation (11) is appealing since it contains only three fitting parameters, each of which has a physical significance: τ is the characteristic growth time of the hole radius at long times, τ_1 is the characteristic decay time for the initial transient behavior, and R_0 is the radius at the beginning of the experiment, corresponding to $t=0$. Equation (11) corresponds to a modification of Eq. (5) such that, at times comparable to or less than τ_1, the term containing τ_1 in Eq. (11) contributes significantly to the value of $R(t)$. At times much greater than τ_1, $R(t)$ in Eq. (11) is dominated by the exponential growth prescribed by τ and is equivalent to Eq. (5).

It is possible to interpret the modification of Eq. (5) resulting in Eq. (11) in terms of a time-dependent viscosity $\eta(t)$. If we allow the time constant τ in Eq. (5) to be time dependent, and combine the result with Eq. (6), we can write

$$R(t) = R_0 \exp\left[\frac{t}{\tau(t)}\right] = R_0 \exp\left[\frac{\epsilon t}{h\eta(t)}\right]. \tag{12}$$

Comparing Eqs. (11) and (12), we obtain an expression for the time-dependent viscosity $\eta(t)$:

$$\eta(t) = \frac{\eta_\infty}{1+\exp(-t/\tau_1)}, \tag{13}$$

where $\eta_\infty=\epsilon\tau/h$ is the viscosity corresponding to times much larger than τ_1. Equation (13) corresponds to a viscosity of $\eta_\infty/2$ at $t=0$ which increases with time to η_∞ with a characteristic time scale τ_1.

The expression for $\eta(t)$ given by Eq. (13) corresponds to a three-parameter spring and dashpot model that can be used to describe a simple viscoelastic fluid. The spring and dashpot model consists of a Voigt element [52,53], which is a parallel arrangement of a spring of modulus E and a dashpot of viscosity η_∞, in series with another dashpot of viscosity η_∞, as shown in Fig. 6 [54,55]. The viscosity of each dashpot is reduced from the zero strain rate value due to shear thinning. During hole growth, surface tension applies a stress $\sigma=2\epsilon/h$ at the edge of the hole. Since hole growth in freely standing films occurs without the accumulation of material around the edge of the hole, but rather with a very small, uniform thickening of the film (see Sec. III B), the stress σ at the edge of the hole effectively remains constant as the holes grow. During the optical microscopy measurements, there are typically a few isolated small ($R<13$ μm) holes present

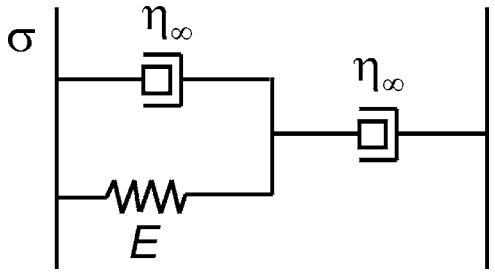

FIG. 6. A spring and dashpot model corresponding to a viscoelastic fluid describing a time-dependent strain $\gamma(t)$ given by Eq. (16): the dashpots have a viscosity η_∞ and the spring has a modulus E.

in the entire film (4 mm in diameter) such that the change in film thickness during the course of the experiment is negligible. We demonstrate that the expression for $\eta(t)$ given in Eq. (13) can be obtained from the simple three parameter spring and dashpot shown in Fig. 6 by applying a constant stress σ across the arrangement of spring and dashpots. The time dependent strain of the Voigt element is [53]

$$\gamma_A(t) = \frac{\sigma}{E}1 - \exp\left(-\frac{E}{\eta_\infty}t\right) \tag{14}$$

and that for the other dashpot is

$$\gamma_B(t) = \frac{\sigma}{\eta_\infty}t. \tag{15}$$

The strains are additive for elements in series leading to an overall time-dependent strain

$$\gamma(t) = \sigma\left[\frac{t}{\eta_\infty} + \frac{1}{E}1 - \exp\left(-\frac{E}{\eta_\infty}t\right)\right] \tag{16}$$

for the three parameter viscoelastic fluid model in Fig. 6. Differentiating Eq. (16) with respect to t, with σ constant, we obtain the time-dependent strain rate

$$\dot{\gamma}(t) = \sigma\left[\frac{1}{\eta_\infty} + \frac{1}{\eta_\infty}1 - \exp\left(-\frac{E}{\eta_\infty}t\right)\right], \tag{17}$$

which results in a time-dependent viscosity equal to

$$\eta(t) = \frac{\sigma}{\dot{\gamma}(t)} = \frac{\eta_\infty}{1 + \exp\left(-\frac{E}{\eta_\infty}t\right)}. \tag{18}$$

Equation (18) is identical to the expression for $\eta(t)$ given in Eq. (13) with $\tau_1 = \eta_\infty/E$. It is perhaps surprising that such a simple model of a viscoelastic fluid, which is characterized by a single relaxation time τ_1, provides excellent fits to the $R(t)$ data obtained for the freely standing PS films in the present study.

In Fig. 7 are shown three representative $R(t)$ data sets and solid curves which were calculated using parameter values corresponding to the best fit of Eq. (11) to the $R(t)$ data sets obtained for freely standing PS films of $M_w = 717 \times 10^3$ for (a) $h = 91$ nm at $T = 101$ °C, (b) $h = 89$ nm at $T = 107$ °C, and (c) $h = 91$ nm at $T = 115$ °C. Excellent fits of Eq. (11) to the

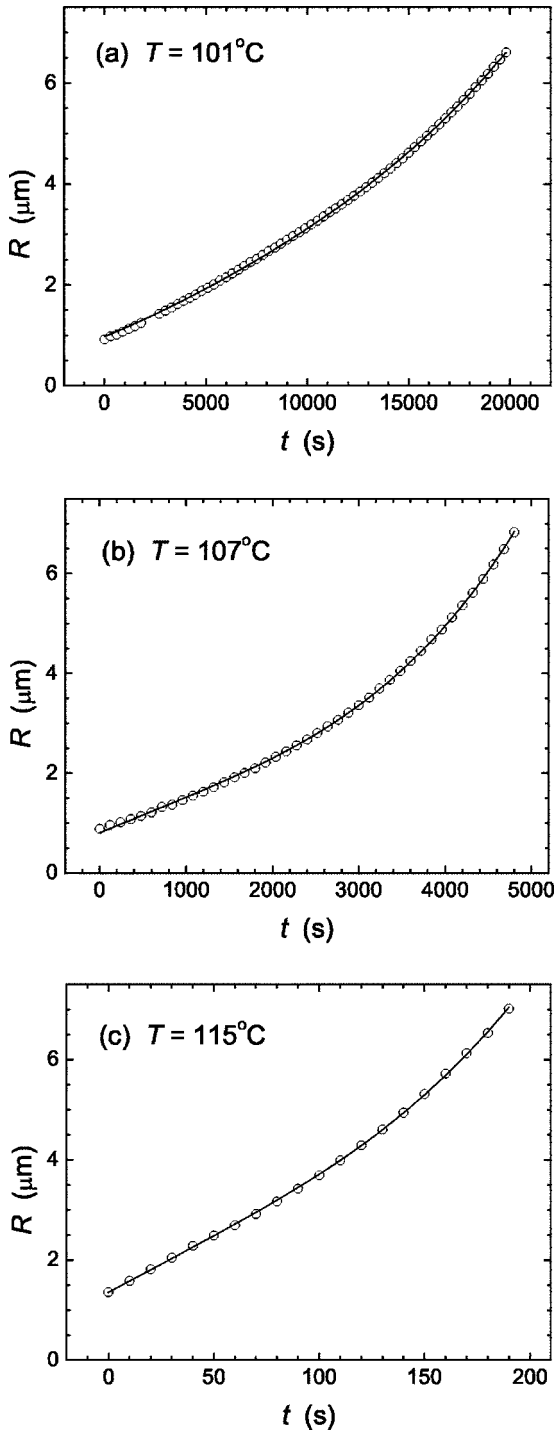

FIG. 7. $R(t)$ data and solid curves corresponding to the best fit of Eq. (11) to the $R(t)$ data for three freely standing PS films of $M_w = 717 \times 10^3$ measured for (a) $h = 91$ nm at $T = 101$ °C, (b) $h = 89$ nm at $T = 107$ °C, and (c) $h = 91$ nm at $T = 115$ °C. The best fit values of τ, τ_1 and R_0 are (a) 11 800±130 s, 10 300±410 s, and 0.97±0.01 μm; (b) 2290±10 s s, 1250±30 s, and 0.81±0.01 μm; and (c) 123±1 s, 69±2 s, and 1.35±0.01 μm.

$R(t)$ data were obtained for all times using the parameter values listed in the caption of Fig. 7, and fits of similar quality were obtained from fits of Eq. (11) to all of the data sets obtained in the present study. The fitted R_0 values ranged

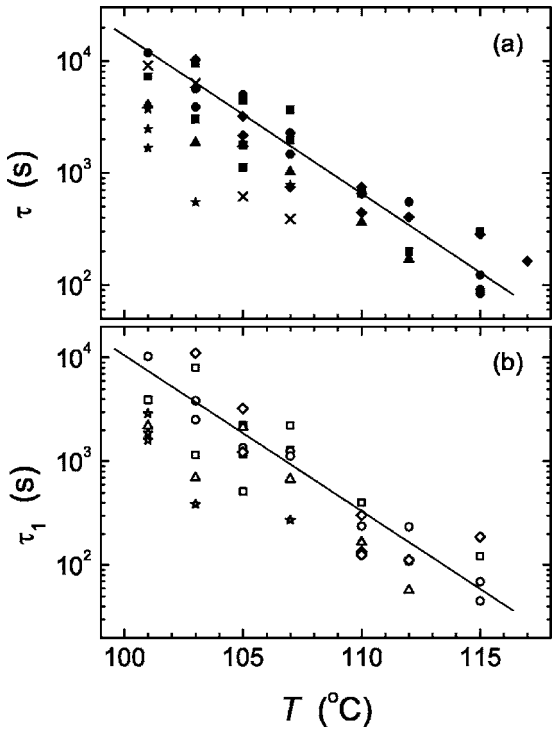

FIG. 8. Best fit values of τ (solid symbols) and τ_1 (open symbols) determined using Eq. (11). τ and τ_1 show a strong and similar temperature dependence (slope of 0.14 for $\log_{10}\tau$ versus T and slope of 0.15 for $\log_{10}\tau_1$ versus T) with $\tau/\tau_1=2.2\pm1.4$. The straight lines correspond to the best fit to the $\log_{10}\tau$ versus T and $\log_{10}\tau_1$ versus T data sets corresponding to the $M_w=717\times10^3$, $h=90$ nm films. The symbols correspond to data for $M_w=120\times10^3$, $h=77$ nm ($\times$); $M_w=282\times10^3$, $h=94$ nm (stars); $M_w=717\times10^3$, $h=61$ nm (triangles); $M_w=717\times10^3$, 90 nm (circles); $M_w=717\times10^3$, $h=125$ nm (diamonds); and $M_w=2240\times10^3$, $h=83$ nm (squares).

from 0.4 to 2.4 μm and were found to be in excellent agreement with the initial values of the hole radius measured at the start of the experiments; the fitted τ values from Eq. (11) were found to be approximately 10% less than those of the characteristic growth times determined by fitting only the exponential growth portion of the data during the late stages of hole growth to Eq. (5) [see Fig. 2(b)]; and τ_1 exhibits the same temperature dependence as τ with $\tau/\tau_1=2.2\pm1.4$. τ_1 decreases with increasing T such that the exponential growth regime is obtained more quickly at higher temperatures in agreement with experimental observations. In Fig. 8 are shown both τ and τ_1, obtained from the fits of Eq. (11) to the $R(t)$ data sets, as a function of temperature where the straight lines correspond to the best linear fits to the $\log_{10}\tau$ versus T data (solid circles) and $\log_{10}\tau_1$ versus T data (open circles) obtained for the $h=90$ nm films of $M_w=717\times10^3$. Because the spread in the $\tau(T)$ and $\tau_1(T)$ data is quite large, no significant differences can be observed between the data sets of different molecular weight and thickness.

B. The shape of the edge of the holes

The shape of the edge of the holes was investigated using atomic force microscopy (AFM). Freely standing PS films in which hole formation had occurred at a fixed temperature for a certain length of time were quenched to room temperature and transferred onto silicon wafers for AFM measurements of the hole edge profile. We found that it was necessary to perform the AFM measurements on films that had been transferred onto silicon because the freely standing films were too susceptible to vibrations to allow high-quality AFM measurements and because the absence of a feedback signal when the AFM tip was within the hole on a freely standing film produced an erratic AFM signal near the edge of the hole. Because the freely standing PS films were quenched to room temperature (75 °C below T_g^{bulk}) before their transfer onto silicon, they should retain the shape of the edge of the hole obtained during hole growth in the freely standing state. We expect that the only modification to the shape of the edge of the hole due to the transfer onto silicon to be a factor of two enhancement of the height of the rim at the edge of the hole, since the edge of the hole in the freely standing PS film is expected to be symmetric with respect to the midplane of the film.

AFM measurements of PS films containing multiple, isolated holes were performed on four films with $M_w=717\times10^3$ and $h=97$ nm in which hole growth had occurred at a measurement temperature of $T=105$ °C or $T=112$ °C for both short and long times. The films quenched after short times contained holes for which only linear $R(t)$ behavior was observed using optical microscopy, while the films quenched after long times contained holes for which exponential $R(t)$ behavior was observed using optical microscopy. There were no significant differences in the profiles of the hole edges between holes growing with linear or exponential $R(t)$ behavior, and in all cases no significant rim was observed at the edge of the hole to within 2 nm (2% of the film thickness). In Fig. 9 are shown AFM height images and corresponding line scans obtained for two PS films heated in the freely standing state to $T=105$ °C for a time t_h, cooled to room temperature with an initial quench rate of ≈10 °C/min immediately after the optical microscopy measurements of $R(t)$, and then transferred onto silicon. Figure 9(a) corresponds to $t_h=25$ min (linear hole growth) and Fig. 9(b) corresponds to $t_h=75$ min (exponential hole growth). In the line scans, it can be seen that there is no significant rim at the edge of the holes.

It has been suggested by Debrégeas *et al.* [37] that the absence of a rim is the result of elastic effects within the film, in which the stress at the edge of the growing hole is transmitted to the rest of the film at the speed of sound. Numerical calculations by Brenner and Gueyffier [36] indicate that the absence of a rim can also result from a purely viscous effect. We note that the absence of a rim is confirmed by applying the equation of continuity for an incompressible fluid $\vec{\nabla}\cdot\vec{v}=0$. If we allow for the possibility of flow normal to the plane of the film (z direction), which should have the form $z(\dot{h}/h)$ from dimensional considerations, in addition to the in-plane flow specified by Eq. (1), then we obtain

$$\vec{\nabla}\cdot\vec{v}=\frac{1}{r}\frac{\partial}{\partial r}(rv)+\frac{\dot{h}}{h}=0, \tag{19}$$

which results in

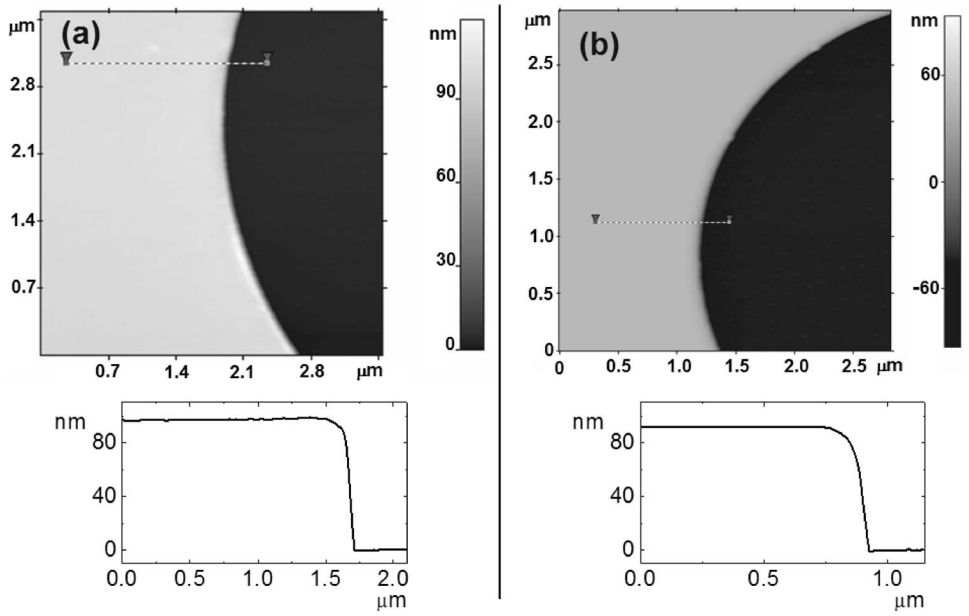

FIG. 9. Atomic force microscopy height images of two freely standing PS films transferred onto silicon after heating for a time t_h at $T=105\ ^\circ\mathrm{C}$ while measuring $R(t)$ using optical microscopy, quenching to room temperature and transferring onto silicon. (a) $t_h=25$ min, corresponding to linear growth of the hole radius, and (b) $t_h=75$ min, corresponding to exponential growth of the hole radius. The lower plots show line scans corresponding to the dashed lines in the AFM images.

$$\frac{\dot{h}}{h}=0, \tag{20}$$

i.e., no change in the film thickness h with time. Equation (20) is valid for holes that are much smaller than the sample size such that the lateral extent of the film can be regarded as infinite, which is a very good approximation for all of the present measurements since the maximum hole radius for all of the hole growth measurements was 13 μm. In the limit of very large holes, the lateral extent of the film cannot be treated as infinite. Given that the fluid velocity must be equal to zero at the maximum radial distance for the film $r=L$, i.e., the edge of the sample, the velocity profile of the fluid is given by [56]

$$v(r)=\frac{\dot{R}R}{L^2-R^2}\left(\frac{L^2}{r}-r\right), \tag{21}$$

which reduces to Eq. (1) for $L\to\infty$. Using Eq. (21) in the equation of continuity [Eq. (19)] gives $h(L^2-R^2)=$constant, which corresponds to an increase in the thickness h which is independent of r as R increases. In previous hole growth measurements in freely standing PS films [32] an increase in the characteristic growth time τ was observed for large holes, which was consistent with an increase in τ due to uniform thickening of the film in accordance with Eq. (6).

In contrast, hole growth in supported polymer films [39,41,42,57–61] necessarily results in the formation of a rim at the edge of the growing hole due to the asymmetric nature of the driving force for hole growth: the surface tension on the top surface is much larger (by a factor of $\sim$10) than the interfacial tension on the bottom interface, which results in an accumulation of material at the edge of the hole on the top of the film [60]. For freely standing films, the driving force due to surface tension is the same for both the top and bottom surfaces which results in a uniform velocity profile across the film, i.e., plug flow [see Eq. (1)].

IV. DISCUSSION

The linear growth of the hole radius with time that is observed during the initial stages of hole growth persists for the longest times at the lowest temperatures used in the present study where elastic effects can contribute significantly. In polymer melts of linear chains, an elastic response of the material is obtained due to the presence of entanglements between the long molecules. According to the theory of reptation [62,63], these entanglements are said to persist for one reptation time τ_d, during which the initial entanglements are lost and new ones are formed. For times longer than τ_d, the material is said to flow, characterized by a viscosity η_0 that scales with the length of the polymer molecules as $\eta_0\sim M_w^{3.4}$. However in the presence of large shear strain rates $\dot{\gamma}>\tau_d^{-1}$, the chains will disentangle rapidly as the constraints surrounding a given chain are removed by the shear strain displacements. New entanglements will not have sufficient time to form as the molecules slip past each other, resulting in a decrease in the density of entanglement points to some steady-state value that is characterized by a reduced viscosity $\eta(\dot{\gamma})$ [45,64]. As described in the Introduction, the tube theory of entangled polymer dynamics can be divided into three different regimes, each characterized by a different dominant relaxation mechanism. The regimes are classified according to the value of the strain rate $\dot{\gamma}$ relative to the reptation (τ_d^{-1}) and Rouse (τ_R^{-1}) rates.

At $T=101\ ^\circ\mathrm{C}$, the shear strain rates $\dot{\gamma}$ measured during our hole growth measurements are of the order of $10^{-4}\ \mathrm{s}^{-1}$ compared to reptation rates of $\tau_d^{-1}\sim 10^{-6}\ \mathrm{s}^{-1}$ to $\sim 10^{-10}\ \mathrm{s}^{-1}$ for the M_w range used in the present study. The values of τ_d for different temperatures were obtained from $J(t)$ data measured for PS melts of $M_w=600\times 10^3$ [52,65] by shifting the $J(t)$ data in time using the temperature shift factor a_T [65]; the τ_d values were then scaled as $M_w^{3.4}$ to obtain values for the different M_w values used in the present study [56]. Rouse times, however, are much more difficult to determine experimentally; thus, we choose to estimate τ_R values using the scaling relation [63]

$$\tau_R = \frac{\tau_d}{3Z}, \tag{22}$$

where $Z=M_w/M_e$ with the entanglement molecular weight $M_e=13\,310$ for PS [66,67]. Equation (22) gives Rouse rates of $\tau_R^{-1} \sim 10^{-4}$ s^{-1} to $\sim 10^{-7}$ s^{-1} at $T=101$ °C. Consequently, we find that the shear strain rates $\dot{\gamma}$ in the present measurements are much larger than τ_d^{-1} and comparable to τ_R^{-1}, indicating that the hole growth measurements are in the intermediate to high shear strain rate regime. The dominant relaxation mechanisms in these regimes are CCR and chain stretch [8,30]. The polymer chains retain their Gaussian conformations on a local scale for shear strain rates $\dot{\gamma}$ less than τ_R^{-1}, with distortions due to chain stretch occurring for larger $\dot{\gamma}$ values. It has been suggested that the effect of chain stretch is less important for shear flows with no rotation, such that the tubes become oriented in the direction of flow, allowing for easier and faster chain retraction along the length of the tube [25,28]. Since the shear flow at the edge of the hole has no rotation [56], CCR is likely the dominant relaxation mechanism, for which the longest relaxation time of the system is of the order of $\dot{\gamma}^{-1}$ [8,21]. If the chain stretch mechanism contributes significantly, it would act to further decrease the longest relaxation time of the system. Thus, a reasonable upper bound on the longest relaxation time is that given by CCR, which is of the order of $\dot{\gamma}^{-1}$. For the hole growth measurements, this implies that the value of τ_1, the measure of the longest relaxation time of the system during hole growth, would be of the order of $\dot{\gamma}^{-1}=\tau/2$ [see Eq. (7)]. We find that the τ and τ_1 values obtained from fits to the experimental data are, on average, related by the ratio $\tau/\tau_1 = 2.2 \pm 1.4$. Thus the linear growth portion observed during the early stages of hole growth is consistent with the decay of entanglements via the CCR mechanism.

In Sec. III A, we showed that excellent fits to the $R(t)$ data were obtained using a time-dependent viscosity [Eq. (13)], which is equivalent to a three-parameter spring and dashpot model (see Fig. 6) characterized by a single relaxation time τ_1. It is perhaps surprising that the behavior of the viscoelastic fluid in the freely standing PS films experiencing shear thinning can be described by a single relaxation time, especially since the description of linear viscoelastic fluids typically requires the use of distributions of relaxation times, corresponding to series arrangements of many Maxwell or Voigt elements [53]. This simplification from a distribution of relaxation times in the linear viscoelastic regime to a single relaxation time in the nonlinear viscoelastic regime may result from the dominance of the CCR mechanism, characterized by a relaxation time determined only by the strain rate.

We consider two effects that may affect the hole growth process in thin freely standing PS films: the possibility of chain scission occuring during hole growth, and the nonequilibrium nature of spincoated polymer films. Since hole growth occurs on time scales less than the reptation time τ_d for all but the lowest molecular weight films, it is important to consider the possibility that the polymer molecules are not able to disentangle on the time scale of the experiment and that the loss in entanglement density occurs by chain scission. This would result in a considerable number of chain segments that are significantly smaller than the original M_w value. Although this effect would not be observed in the hole growth experiment at long times, since the viscosity is independent of M_w in the shear thinning regime [68], it might affect the transient behavior. We expect that chain scission is unlikely based on crazing measurements by Berger and Kramer [69] of PS films ($h=700$ nm) with M_w values ranging from 233×10^3 to 3×10^6 performed at temperatures less than T_g ($20\ °\text{C} < T < 90\ °\text{C}$). During crazing, large voids that are 20 to 30 nm in width form in the polymer material separated by fibrils that are typically 4 to 10 nm in width [70]. Berger and Kramer estimated that the formation of the oriented craze fibrils necessitates the destruction of nearly 50% of the entanglement network, which can occur by either chain scission or chain disentanglement. The molecular weight dependence of the extension ratio in the craze was measured at temperatures from 20 to 90 °C, and was found to be independent of M_w or strain rate $\dot{\gamma}$, which is expected for entanglement loss by chain scission, until some threshold temperature was reached. For $M_w=1.8\times10^6$ films, the extension ratio remained constant until a temperature of $T=70$ °C for $\dot{\gamma}=4.1\times10^{-6}$ s^{-1} and $T=90$ °C for $\dot{\gamma}\sim10^{-2}$ s^{-1}. For higher temperatures, the disentanglement times were estimated and found to scale with molecular weight as $M_w^{2.9\pm0.5}$. This was believed to be strong evidence indicating that the entanglement loss was due to chain disentanglement via reptation. The hole growth measurements presented in this paper were performed at higher temperatures ($101\ °\text{C} < T < 117\ °\text{C}$) with comparable M_w values and strain rates ($1.5\times10^{-4}\ \text{s}^{-1} < \dot{\gamma} < 2\times10^{-2}\ \text{s}^{-1}$) than those used for Berger and Kramer's crazing study. Thus it seems that sufficient mobility exists for the chains to disentangle at the temperatures and strain rates of the present study even though the hole growth times are less than the reptation time τ_d, and it is unlikely that chain scission occurs during the hole growth measurements of the present study.

Second, we consider the effect of the spincoating process used to deposit thin polymer films. In the spincoating process, a dilute solution of polymer dissolved in a good solvent is dropped onto a spinning substrate. The solvent molecules evaporate rapidly, with the glassy state "freezing in" below a critical solvent concentration, which for PS in toluene at 25 °C is 14% by mass of toluene [71]. This means that the material undergoes a large shrinkage in the glassy state as the remaining solvent molecules are removed. Additionally, the high spin speeds can lead to radial alignment of the chains. The net effect is likely to produce a density of entanglements of the molecules that is less than that observed in bulk, as inferred in recent Fourier-transform infrared spectroscopy (FTIR) measurements on spincoated, thin ($h<200$ nm) freely standing PS films of $M_w=200\times10^3$ [72]. We can estimate the reduction in the density of entanglements of the spincoated film by assuming that it is equivalent to that of the polymer solution when the glassy state "freezes in." The molecular weight of the chain segments between entanglement points M_e in a solution is that of the melt divided by the polymer volume fraction ϕ: $M_e^{\text{soln}} \sim M_e^{\text{melt}}/\phi$ [45,73]. Therefore we expect that the density of entanglements is reduced

by about 16% in a PS film just after spincoating deposition compared to that in bulk. Even though the PS films on mica substrates are heated in vacuum to a temperature $T = 115\ ^\circ\mathrm{C}$, which is greater than T_g^{bulk}, this procedure is not necessarily sufficient to relax the chains fully since segments of the chains may be pinned to the underlying substrate. In addition, for the time and temperature used for heating the PS films on mica in the present study, the films with the two largest M_w values have been heated for times significantly shorter than the reptation time τ_d, whereas films with the two smallest M_w values have been heated for times much longer than τ_d. Therefore it might be expected that the degree of equilibration is different for PS films of different M_w values used in the present study, with the highest M_w films being furthest from equilibrium. For hole growth occurring at long times corresponding to the shear thinning regime, the reduction in entanglements produced by the shear strain rate is expected to be large, producing large reductions in the viscosity (see Fig. 3), such that the initial arrangement of polymer molecules in the films should not be important. This decrease in entanglement density will occur on a time scale corresponding to the renewal of the initial set of entanglements, i.e., the longest relaxation time of the system, which in the case of the present hole growth measurements is of the order of $\dot{\gamma}^{-1} = \tau/2$ for the CCR relaxation mechanism and is much smaller than the reptation time τ_d. Because such a large change in the entanglement density occurs over a relatively short time τ_1, which does not have a strong M_w dependence (see Fig. 8), it is unlikely that the nonequilibrium nature of the PS freely standing films due to spincoating significantly affects the hole growth process.

V. CONCLUSIONS

We have performed hole growth measurements in freely standing polystyrene films using optical microscopy and we observed a change from linear growth of the hole radius with time to exponential growth of the hole radius with time as time proceeds. We found that the exponential growth regime was consistent with viscous flow of the polymer with a reduced viscosity at the edge of the hole due to the large shear strain rates present during hole growth. The $R(t)$ data were well fit by an expression for exponential growth of the hole radius which is modified to incorporate a time-dependent viscosity $\eta(t)$. The characteristic time τ_1, which describes the decay of the initial transient behavior before the exponential growth regime is reached, is attributed to the decay of entanglements and is found to scale with the hole growth time τ which is consistent with the convective constraint release (CCR) relaxation mechanism of the tube theory of entangled polymer dynamics. The authors hope that the detailed hole growth measurements presented in this manuscript, probing the shear deformation of linear monodisperse polystyrene melts with different molecular weights at high shear rates in a simple planar, radially symmetric geometry, will provide a good test case for the tube theory of entangled polymer dynamics and the available constitutive equations.

ACKNOWLEDGMENTS

We wish to thank Dr. Oleg Stukalov for assistance with the atomic force microscopy measurements. Financial support from the Natural Sciences and Engineering Research Council (NSERC) of Canada and the Province of Ontario (PREA program) is gratefully acknowledged.

[1] T. P. Lodge, N. A. Rotstein, and S. Prager, Adv. Chem. Phys. **79**, 1 (1990).
[2] M. Doi and S. F. Edwards, J. Chem. Soc., Faraday Trans. 2 **74**, 1789 (1978).
[3] M. Doi and S. F. Edwards, J. Chem. Soc., Faraday Trans. 2 **74**, 1802 (1978).
[4] M. Doi and S. F. Edwards, J. Chem. Soc., Faraday Trans. 2 **74**, 1818 (1978).
[5] M. Doi and S. F. Edwards, J. Chem. Soc., Faraday Trans. 2 **75**, 38 (1979).
[6] S. F. Edwards, Proc. Phys. Soc. London **92**, 9 (1967).
[7] P.-G. de Gennes, J. Chem. Phys. **55**, 572 (1971).
[8] T. C. B. McLeish, Adv. Phys. **51**, 1379 (2002).
[9] H. Watanabe, Prog. Polym. Sci. **24**, 1253 (1999).
[10] L. G. Leal and J. P. Oberhauser, Korea-Aust. Rheol. J. **12**, 1 (2000).
[11] M. Doi, J. Polym. Sci., Polym. Chem. Ed. **21**, 667 (1983).
[12] D. S. Pearson and E. Helfand, Macromolecules **17**, 888 (1984).
[13] S. T. Milner and T. C. B. McLeish, Macromolecules **30**, 2159 (1997).
[14] S. T. Milner and T. C. B. McLeish, Macromolecules **31**, 7479 (1998).
[15] S. T. Milner and T. C. B. McLeish, Phys. Rev. Lett. **81**, 725 (1998).
[16] M. Rubinstein and R. H. Colby, J. Chem. Phys. **89**, 5291 (1988).
[17] J. L. Viovy, M. Rubinstein, and R. H. Colby, Macromolecules **24**, 3587 (1991).
[18] S. T. Milner, J. Rheol. **40**, 303 (1996).
[19] G. Marrucci, J. Non-Newtonian Fluid Mech. **62**, 279 (1996).
[20] G. Ianniruberto and G. Marrucci, J. Non-Newtonian Fluid Mech. **65**, 241 (1996).
[21] D. W. Mead, R. G. Larson, and M. Doi, Macromolecules **31**, 7895 (1998).
[22] G. Ianniruberto and G. Marrucci, Proc. Int. Congr. Rheol. **2**, 102 (2000).
[23] A. E. Likhtman, S. T. Milner, and T. C. B. McLeish, Phys. Rev. Lett. **85**, 4550 (2000).
[24] S. T. Milner, T. C. B. McLeish, and A. E. Likhtman, J. Rheol. **45**, 539 (2001).
[25] G. Marrucci and N. Grizzuti, Gazz. Chim. Ital. **118**, 179 (1988).
[26] D. Pearson, E. Herbolzheimer, N. Grizzuti, and G. Marrucci, J. Polym. Sci., Part B: Polym. Phys. **29**, 1589 (1991).
[27] D. W. Mead and L. G. Leal, Rheol. Acta **34**, 339 (1995).
[28] D. W. Mead, D. Yavich, and L. G. Leal, Rheol. Acta **34**, 360 (1995).

[29] V. Mhetar and L. A. Archer, J. Non-Newtonian Fluid Mech. **81**, 71 (1999).
[30] R. S. Graham, A. E. Likhtman, T. C. B. McLeish, and S. T. Milner, J. Rheol. **47**, 1171 (2003).
[31] J. Bent *et al.*, Science **301**, 1691 (2003).
[32] K. Dalnoki-Veress, B. G. Nickel, C. Roth, and J. R. Dutcher, Phys. Rev. E **59**, 2153 (1999).
[33] J. N. Israelachvili, *Intermolecular & Surface Forces*, 2nd ed. (Academic, San Diego, 1991).
[34] F. E. C. Culick, J. Appl. Phys. **31**, 1128 (1960).
[35] W. E. Ranz, J. Appl. Phys. **30**, 1950 (1959).
[36] M. P. Brenner and D. Gueyffier, Phys. Fluids **11**, 737 (1999).
[37] G. Debrégeas, P. Martin, and F. Brochard-Wyart, Phys. Rev. Lett. **75**, 3886 (1995).
[38] G. Debrégeas, P.-G. de Gennes, and F. Brochard-Wyart, Science **279**, 1704 (1998).
[39] G. Reiter, Phys. Rev. Lett. **87**, 186101 (2001).
[40] G. Reiter, Eur. Phys. J. E **8**, 251 (2002).
[41] G. Reiter, M. Sferrazza, and P. Damman, Eur. Phys. J. E **12**, 133 (2003).
[42] P. Damman, N. Baudelet, and G. Reiter, Phys. Rev. Lett. **91**, 216101 (2003).
[43] J. H. Xavier, Y. Pu, C. Li, M. H. Rafailovich, and J. Sokolov, Macromolecules **37**, 1470 (2004).
[44] G. T. Dee and B. B. Sauer, J. Colloid Interface Sci. **152**, 85 (1992).
[45] W. W. Graessley, Adv. Polym. Sci. **16**, 1 (1974).
[46] C. B. Roth, B. G. Nickel, J. R. Dutcher, and K. Dalnoki-Veress, Rev. Sci. Instrum. **74**, 2796 (2003).
[47] C. B. Roth and J. R. Dutcher, the following paper, Phys. Rev. E **72**, 021803 (2005).
[48] A. E. Likhtman and T. C. B. McLeish, Macromolecules **35**, 6332 (2002).
[49] R. Bird and J. Wiest, Annu. Rev. Fluid Mech. **27**, 169 (1995).
[50] J. A. Forrest, K. Dalnoki-Veress, and J. R. Dutcher, Phys. Rev. E **56**, 5705 (1997).
[51] J. D. Gunton, M. S. Miguel, and P. S. Sahni, in *Phase Transitions and Critical Phenomena*, edited by C. Domb and J. L. Lebowitz (Academic Press, London, 1983), Vol. 8.
[52] J. D. Ferry, *Viscoelastic Properties of Polymers*, 3rd ed. (John Wiley & Sons, New York, 1980).
[53] I. M. Ward, *Mechanical Properties of Solid Polymers*, 2nd ed. (John Wiley & Sons, New York, 1983).
[54] W. N. Findley, J. S. Lai, and K. Onaran, *Creep and Relaxation of Nonlinear Viscoelastic Materials with an Introduction to Linear Viscoelasticity* (North-Holland Publishing Company, Amsterdam, 1976).
[55] G. M. Kamath and N. M. Wereley, Smart Mater. Struct. **6**, 351 (1997).
[56] C. B. Roth, Ph.D. thesis, University of Guelph, Guelph, Ontario, Canada, 2004.
[57] R. Seemann, S. Herminghaus, and K. Jacobs, J. Phys.: Condens. Matter **13**, 4925 (2001).
[58] P. Müller-Buschbaum, J. Phys.: Condens. Matter **15**, R1549 (2003).
[59] Special issue on "Unstable Thin Films," Eur. Phys. J. E **12**, 359 (2003).
[60] F. Brochard-Wyart, G. Debrégeas, R. Fondecave, and P. Martin, Macromolecules **30**, 1211 (1997).
[61] K. Jacobs, R. Seemann, G. Schatz, and S. Herminghaus, Langmuir **14**, 4961 (1998).
[62] P.-G. de Gennes, *Scaling Concepts in Polymer Physics* (Cornell University Press, Ithaca, NY, 1979).
[63] M. Doi and S. F. Edwards, *The Theory of Polymer Dynamics* (Oxford University Press, Oxford, 1986).
[64] W. W. Graessley, J. Chem. Phys. **47**, 1942 (1967).
[65] D. J. Plazek and V. M. O'Rourke, J. Polym. Sci., Part A-2 **9**, 209 (1971).
[66] L. J. Fetters, D. J. Lohse, D. Richter, T. A. Witten, and A. Zirkel, Macromolecules **27**, 4639 (1994).
[67] L. J. Fetters, D. J. Lohse, and W. W. Graessley, J. Polym. Sci., Part B: Polym. Phys. **37**, 1023 (1999).
[68] R. A. Stratton, J. Colloid Interface Sci. **22**, 517 (1966).
[69] L. L. Berger and E. J. Kramer, Macromolecules **20**, 1980 (1987).
[70] E. J. Kramer, Adv. Polym. Sci. **52/53**, 1 (1983).
[71] G. B. McKenna, J. Phys. IV **10**, 53 (2000).
[72] O. N. Tretinnikov and R. G. Zbankov, Macromolecules **37**, 3543 (2004).
[73] B. B. Sauer and D. J. Walsh, Macromolecules **27**, 432 (1994).
[74] K. Dalnoki-Veress, J. A. Forrest, C. Murray, C. Gigault, and J. R. Dutcher, Phys. Rev. E **63**, 031801 (2001).